

Supernova neutrino scattering off Gadolinium even isotopes in water Cherenkov detectors.

Paraskevi C. Divari

*Department of Physical Sciences and Applications,
Hellenic Military Academy, Vari 16673, Attica, Greece*

Neutrinos in water can be detected thanks to several reactions. The most important one is the inverse beta decay $\bar{\nu}_e + p \rightarrow n + e^+$. The detection of 2.2 MeV γ from neutron capture on free protons is very difficult. The feasibility of Gadolinium (Gd) doping in water Cherenkov detectors essentially reduces background signals and enhances the sensitivity to neutrino detection. In this work the supernova neutrino charged-current interactions with the most abundant Gd even isotopes (A=156,158 and 160) are studied. We use measured spectra and the quasiparticle random phase approximation to calculate the charged current response of Gd isotopes to supernova neutrinos. Flux-averaged cross sections are obtained considering quasi-thermal neutrino spectra.

PACS numbers: 26.50.+x, 13.15.+g, 25.30.Pt, 28.20.-V

I. INTRODUCTION

A number of detectors like water Cherenkov detectors (WCDs) [1–3], have been used in various neutrino detection experiments. They have the ability to detect either the charged-current ν_e ($\bar{\nu}_e$) interaction, which produces electrons (positrons), or the neutral current interaction (for all flavors), which usually results in the production of neutrons and photons, or both. The sensitivity of the detectors can be enhanced through either building a larger water tank that increases the probability of neutrino interaction in WCD, or including additives, such as gadolinium (Gd), in water that essentially reduces background signals [4]. Neutrinos in water can be detected thanks to several reactions. The most important are the following three:

1. inverse beta decay (IBD): $p + \bar{\nu}_e \rightarrow n + e^+$
2. elastic scattering on electrons : $\nu + e^- \rightarrow \nu + e^-$
3. neutral current scattering on oxygen : $\nu + {}^{16}\text{O} \rightarrow \nu + {}^{16}\text{O}^*$

with $\nu = \nu_e, \bar{\nu}_e, \nu_{\mu,\tau}, \bar{\nu}_{\mu,\tau}$

WCDs are primarily sensitive to $\bar{\nu}_e$'s through IBD. The positron produced by IBD emits Cherenkov light, which is detected by a photomultiplier tube (PMT) array placed around the detection volume. Due to Cherenkov threshold the detection of the 2.2 MeV γ from neutron capture on hydrogen nucleus ($n + p \rightarrow d + \gamma$ (2.2 MeV)) is very difficult. It is possible to dissolve Gd compounds in the water to enhance neutron tagging and allow the IBD and electron elastic scattering signals to be separated [4, 5]. The large neutron capture cross section of Gd allows neutrons formed in IBD events to be quickly ($\sim 20\mu\text{s}$) captured, emitting three to four gamma rays with a total energy of 8 MeV ($n + \text{Gd} \rightarrow \text{Gd}^* + \gamma$ (8 MeV)) in close time and space coincidence with the positron. In Super-Kamiokande (SK), which is a 22.5 kton (fiducial) WCD, it has been found that [4, 5] with 0.2% (by mass) Gd added to SK, $\sim 90\%$ of the IBD events could be tagged. The remaining IBD events as well as the $\bar{\nu}_e$ absorption events on ${}^{16}\text{O}$ can then be statistically subtracted from the remaining signal.

Future extremely large WCDs like Hyper-Kamiokande (560 kton fiducial) would have a dramatic impact on detecting supernova or solar neutrinos using the Gd-doping technique. Therefore, it would be interesting to draw our attention to the possibility of calculating the cross sections for low-energy neutrinos on Gd isotopes. In the present work we pay special attention on calculations of charged current (CC) neutrino/antineutrino-Gd cross sections at neutrino energies below 100 MeV, considering the most abundant even isotopes of Gadolinium that is, isotopes with mass number A=156,158 and 160 (20.47%, 24.84% and 21.86% abundant, respectively). The corresponding nuclear matrix elements have been calculated in the framework of quasi-particle random phase approximation (QRPA) [6–8].

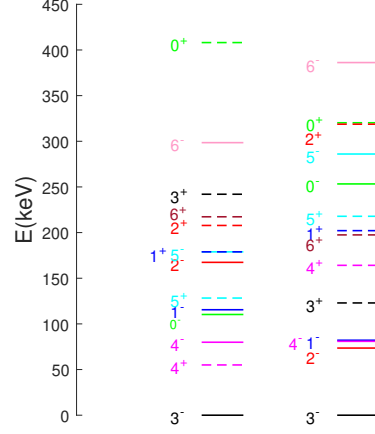


FIG. 1: (Color on line) Experimental (left)[9] and theoretical (right) spectra of ^{158}Tb

II. BRIEF DESCRIPTION OF THE FORMALISM

The standard model effective Hamiltonian in the charged current reactions

$$\begin{aligned} (A, Z) + \nu_e &\rightarrow (A, Z + 1) + e^- \\ (A, Z) + \bar{\nu}_e &\rightarrow (A, Z - 1) + e^+ \end{aligned}$$

can be written

$$\mathcal{H} = \frac{G_F \cos\theta_c}{\sqrt{2}} j_\mu(\mathbf{x}) J^\mu(\mathbf{x}), \quad (1)$$

$A(Z)$ represents the mass(proton) number of a nucleus, respectively. Here $G_F = 1.1664 \times 10^{-5} \text{GeV}^{-2}$ denotes the Fermi weak coupling constant and $\theta_c \simeq 13^\circ$ is the Cabibbo angle. According to V-A theory, the leptonic current takes the form [10–13]

$$j_\mu = \bar{\psi}_{\nu_\ell}(x) \gamma_\mu (1 - \gamma_5) \psi_{\nu_\ell}(x), \quad (2)$$

where ψ_{ν_ℓ} are the neutrino/antineutrino spinors. The hadronic current of vector, axial-vector and pseudo-scalar components is written as

$$\begin{aligned} J_\mu = \bar{\Psi}_N [&F_1(q^2) \gamma_\mu + F_2(q^2) \frac{i\sigma_{\mu\nu} q^\nu}{2M_N} + F_A(q^2) \gamma_\mu \gamma_5 \\ &+ F_P(q^2) \frac{1}{2M_N} q_\mu \gamma_5] \Psi_N \end{aligned} \quad (3)$$

(M_N stands for the nucleon mass, Ψ_N denotes the nucleon spinors and q^2 , the square of the four-momentum transfer). By the conservation of the vector current (CVC), the vector form factors $F_{1,2}(q^2)$ can be written in terms of the proton and neutron electromagnetic form factors [14]. The axial-vector form factor $F_A(q^2)$ is assumed to be of dipole form [15] while the pseudoscalar form factor $F_P(q^2)$ is obtained from the Goldberger-Treiman relation [10].

In the convention we used in the present work the square of the momentum transfer, is written as

$$q^2 = q^\mu q_\mu = \omega^2 - \mathbf{q}^2 = (\varepsilon_i - \varepsilon_f)^2 - (\mathbf{p}_i - \mathbf{p}_f)^2, \quad (4)$$

where $\omega = \varepsilon_i - \varepsilon_f$ is the excitation energy of the final nucleus. $\varepsilon_i(\mathbf{p}_i)$ denotes the energy(3-momenta) of the incoming neutrino/antineutrino and $\varepsilon_f(\mathbf{p}_f)$ those of the outgoing electron/positron, respectively. The charged-current

neutrino/antineutrino-nucleus cross section is written as [11]

$$\sigma(\varepsilon_i) = \frac{2G_F^2 \cos^2 \theta_c}{2J_i+1} \sum_f |\mathbf{p}_f| \varepsilon_f \int_{-1}^1 d(\cos \theta) F(\varepsilon_f, Z_f) \times \left(\sum_{J=0}^{\infty} \sigma_{CL}^J(\theta) + \sum_{J=1}^{\infty} \sigma_T^J(\theta) \right) \quad (5)$$

θ denotes the lepton scattering angle. The summations in Eq. (5) contain the contributions σ_{CL}^J , for the Coulomb $\widehat{\mathcal{M}}_J$ and longitudinal $\widehat{\mathcal{L}}_J$, and σ_T^J , for the transverse electric $\widehat{\mathcal{T}}_J^{el}$ and magnetic $\widehat{\mathcal{T}}_J^{mag}$ multipole operators defined as in Ref. [6]. These operators include both polar-vector and axial-vector weak interaction components.

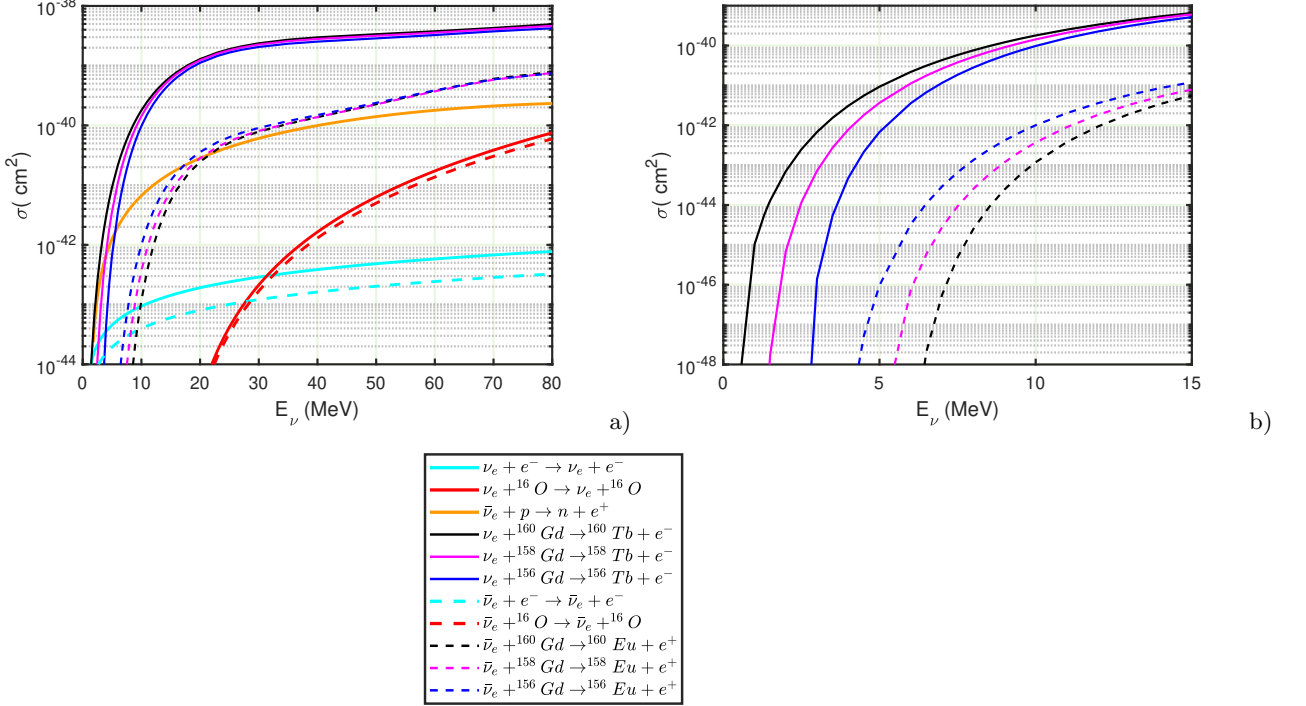


FIG. 2: (Color on line) (a) Total cross sections for ν_e and $\bar{\nu}_e$ Gd interactions. Also presented are total cross sections for inverse beta decay, elastic scattering on electrons and neutral current scattering on oxygen. (b) Total cross sections for ν_e and $\bar{\nu}_e$ Gd interactions in the energy region from 0 to 15 MeV.

III. NEUTRINO SPECTRA

Energy distributions of supernova neutrinos are shaped by the circumstances in which the neutrinos are emitted. Neutrinos leaving the star are responsible for the cooling of the proto-neutron star forming in the stars core. Hence, their spectrum resembles a thermal one, with temperatures reflecting the conditions at the site where they decoupled. However, the fact that different kinds of neutrinos are involved in different interactions, and that the reactivity of the neutrino/antineutrino depends on its energy, flavor, and helicity, modulates this picture. For all neutrino/antineutrino flavors, the energies are in the range of a few to a few tens of MeV, although calculations of neutrino transport that use different opacities achieve somewhat different spectra.

There are different ways to characterize the spectra of the neutrino time integrated fluxes emerging from a Supernova (SN). Recent results showed the supernova-neutrino energy distribution to be accurately parameterized with a power-law distribution [16, 17]:

$$\eta_{PL}(E_\nu) = \frac{E_\nu^{\alpha_i} e^{-E_\nu/T_i}}{T_i^{\alpha_i+1} \Gamma(\alpha_i + 1)} \quad (6)$$

adopting the Keil parametrization [18] for the neutrino fluence

$$\mathcal{F}_i^0(E_\nu) = \frac{dF_i^0}{dE_\nu} = \left(\frac{\mathcal{E}_i}{\langle E_i \rangle 4\pi D^2} \right) \eta_{PL}(E_\nu) \quad (7)$$

with $i = \nu_e, \bar{\nu}_e, \nu_x$, $\nu_x = \nu_{\mu,\tau}, \bar{\nu}_{\mu,\tau}$, where E_ν is the neutrino energy, $\Gamma(x)$ the Euler gamma function, T_i the temperature

$$T_i = \frac{\langle E_i \rangle}{(\alpha_i + 1)}, \quad (8)$$

$\langle E_i \rangle$ being the mean energy and α_i a parameter called the pinching parameter that relates to the width of the spectrum. Typically α_i takes the values $2.5 - 5$ for time dependent flux [18] depending on the flavor and the phase of neutrino emission. Eq. (7) is observed to be closer to thermal distribution than the time-dependent flux. A reasonable conservative interval for α is [19] $1.5 \leq \alpha \leq 3.5$. \mathcal{E}_i denotes the total energy in that i flavor and D is the distance to the supernova. A SN at a distance $D = 10\text{kpc}$ emits total energy $\approx 3 \times 10^{53}$ erg over a burst $\Delta t \approx 10\text{s}$ in neutrinos of all six flavors [20–22]. The $\nu_x = \{\nu_{\mu,\tau}, \bar{\nu}_{\mu,\tau}\}$ have similar interactions and thus similar average energies and fluences. Therefore, the total energy is divided as $\mathcal{E} = \mathcal{E}_{\nu_e} + \mathcal{E}_{\bar{\nu}_e} + 4\mathcal{E}_{\nu_x}$. In typical SN simulations the equipartition hypothesis among the primary flavors is taken $\mathcal{E}_{\nu_e} \approx \mathcal{E}_{\bar{\nu}_e} \approx \mathcal{E}_{\nu_x} = 5 \times 10^{52}\text{erg}$.

According to the simulations in [17] and the findings from the SN1987A [23, 24], the average energy for the electron antineutrino can be set to $\langle E_{\bar{\nu}_e} \rangle = 12\text{ MeV}$. The mean energy of the non-electronic species ν_x can be taken 30% higher than the one of the $\bar{\nu}_e$ that is $\langle E_{\nu_x} \rangle = 15.6\text{ MeV}$ compatible with what is found in [18]. The electron neutrino mean energy can be taken from the condition that the proton (or electron) fraction of the iron core in the neutron star forming is 0.4 which gives $\langle E_{\nu_e} \rangle = 9.5\text{ MeV}$ [16].

IV. RESULTS

The nuclear matrix elements entering in Eq. (5) have been calculated in the framework of pnQRPA. The target isotopes $^{156,158,160}\text{Gd}$ were assumed to be at the BCS ground state (initial state). The final excited states $|J_f^\pi\rangle$ of $^{156,158,160}\text{Tb}$ ($^{156,158,160}\text{Eu}$) isotopes have been calculated by solving the pnQRPA equations [6]. The active model space for protons consists of the complete oscillator shells $4\hbar\omega$ and $5\hbar\omega$ while for neutrons the oscillator shells $5\hbar\omega$ and $6\hbar\omega$. The corresponding single particle energies (s.p.e) were produced by the well known Coulomb corrected Woods-Saxon potential adopting the parameters of Bohr and Mottelson [25]. The quality of the obtained results could be improved adjusting some of the proton and neutron single particle energies. These adjustments are presented in Table I.

TABLE I: Adjusted (Adj) single-particle energies together with the Woods-Saxon(WS) energies (in MeV) for the neutron (n) and proton (p) orbitals.

orbital	^{156}Gd		^{158}Gd		^{160}Gd	
	WS	Adj	WS	Adj	WS	Adj
$n\ 1f_{7/2}$	-6.43	-6.10	-6.40	-6.07	-6.37	-6.03
$n\ 0h_{9/2}$	-5.68	-5.00	-5.71	-5.03	-5.73	-5.05
$n\ 0h_{11/2}$	-11.05	-6.00	-10.99	-5.94	-10.93	-5.87
$p\ 0h_{11/2}$	-5.43	-5.00	-6.01	-5.58	-6.58	-6.14

The two-body matrix elements were obtained from the Bonn one-boson-exchange potential applying the G-matrix techniques [26]. Pairing interaction between the nucleons can be adjusted by solving the BCS equations. Specifically, the monopole matrix elements of the two-body interaction are scaled by the pairing-strength parameters g_{pair}^p (for protons) and g_{pair}^n (for neutrons) in such a way that the resulting lowest quasiparticle energy to reproduce the phenomenological pairing gap $\Delta_{p,n}^{exp}$ [27]. In Table II the values of the pairing-strength parameters, as well as the theoretical energy gaps ($\Delta_{p,n}^{th}$) determined at the BCS level are tabulated. Also listed is the oscillator length parameter b for each isotope as well as their corresponding natural abundances. In the pnQRPA calculations the interaction

TABLE II: Pairing-strength parameters for protons (g_{pair}^p) and neutrons (g_{pair}^n) determined by solving iteratively the BCS equations. They are fixed in such a way that the corresponding experimental energy gaps (in MeV) for protons (Δ_p^{exp}) and neutrons (Δ_n^{exp}) to be reproduced. The values of the harmonic oscillator size parameter b as well as the corresponding natural abundances for each isotope are also shown.

isotope	Abundance (%)	b(fm)	g_{pair}^n	g_{pair}^p	Δ_p^{th}	Δ_p^{exp}	Δ_n^{th}	Δ_n^{exp}
^{156}Gd	20.5	2.319	0.75	0.80	0.960	0.961	1.09	1.069
^{158}Gd	24.8	2.324	0.80	0.77	0.881	0.879	1.08	0.893
^{160}Gd	21.8	2.328	0.81	0.78	0.884	0.857	1.05	0.831

matrix elements were scaled separately for each multipole state. In this way the lowest excitation energy of each multipole was brought as close as possible to the experimental energy spectra. As an example in Fig. 1 the calculated energy spectrum of ^{158}Tb together with the experimental one [9] is presented.

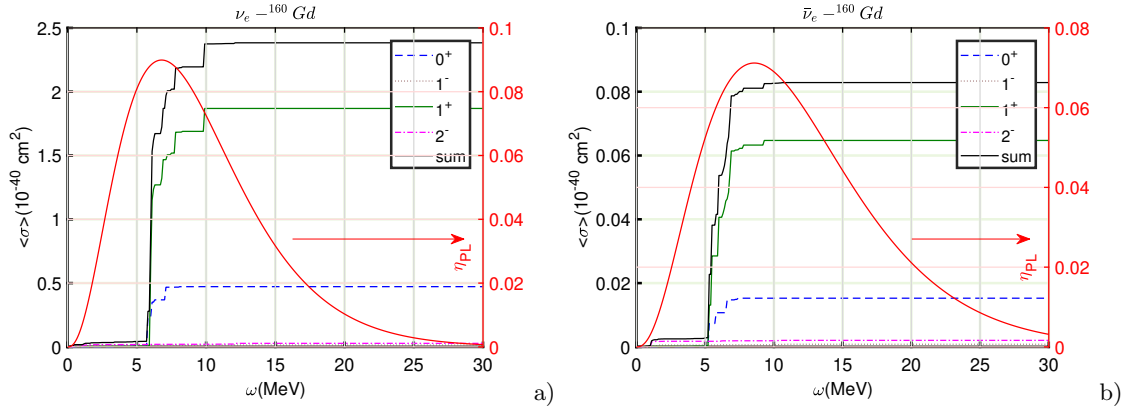


FIG. 3: (Color on line) Cumulative flux-averaged cross sections (in units 10^{-40}cm^2) as a function of excitation energy ω for the reactions $^{160}\text{Gd}(\nu_e, e^-)^{160}\text{Tb}$ and $^{160}\text{Gd}(\bar{\nu}_e, e^+)^{160}\text{Eu}$. Both multipole state contribution of $J = 0^+, 1^+, 1^-, 2^-$ and the total sum are presented. The power-law(PL) distributions η_{PL} (red solid line) for $\langle E_{\nu_e} \rangle = 9.5\text{MeV}$ (a) and $\langle E_{\bar{\nu}_e} \rangle = 12\text{MeV}$ (b) with $\alpha = 2.5$ are also displayed.

In Fig. 2(a) we present the numerical results of the total scattering cross section $\sigma(E_\nu)$ given by Eq. (5) as a function of the incoming neutrino energy E_ν for the reactions $^A\text{Gd}(\nu_e, e^-)^A\text{Tb}$ and $^A\text{Gd}(\bar{\nu}_e, e^+)^A\text{Eu}$, $A=156, 158, 160$ respectively. The Q values ($Q = M(A, Z \pm 1) - M(A, Z)$) of the reactions are given in Table III. The overall cross

TABLE III: Q values (in MeV) for the corresponding neutrino-nucleus interactions.

	$\nu_e-^{156}\text{Gd}$	$\bar{\nu}_e-^{156}\text{Gd}$	$\nu_e-^{158}\text{Gd}$	$\bar{\nu}_e-^{158}\text{Gd}$	$\nu_e-^{160}\text{Gd}$	$\bar{\nu}_e-^{160}\text{Gd}$
Q (MeV)	2.444	2.449	1.219	3.487	0.106	4.579

sections $\sigma(E_\nu)$ includes a summation over transitions to all possible final states characterized by multipoles up to $J^\pi = 6^\pm$. Here we have considered a hybrid prescription already used in previous calculations [6, 28, 29], where Fermi function for Coulomb correction is used below the energy region on which both approaches predict the same values, while EMA is adopted above this energy region. As it is seen, both the neutrino and antineutrino cross sections increase strongly with increasing neutrino energy while the ν_e -nucleus cross sections are about an order of magnitude greater than the corresponding antineutrino ones. For comparison in Fig. 2(a) we also present the total cross sections for inverse beta decay, elastic scattering on electrons and neutral current scattering on oxygen. For clarity figure 2(b) plots the energy cross sections for $\nu_e - \text{Gd}$ and $\bar{\nu}_e - \text{Gd}$ reactions in the energy region 0 to 15 MeV.

TABLE IV: Fraction (in %) of the flux-averaged cross section associated to states of a given multipolarity with respect to the total flux-averaged cross section, i.e. $\langle\sigma\rangle_{J^\pi}/\langle\sigma\rangle_{tot}$. Results are given for all positive and negative states having total angular momentum J between 0 and 3. The first column gives the considered neutrino nucleus reaction and the second one the corresponding mean energy $\langle E_\nu \rangle$. The last column give the total flux-averaged cross sections in units of 10^{-42} cm^2 . The pinching parameter is taken to be $\alpha = 2.5$.

	$\langle E_\nu \rangle (\text{MeV})$	0^+	1^+	2^+	3^+	0^-	1^-	2^-	3^-	$\langle\sigma\rangle (10^{-42} \text{ cm}^2)$ $E_{th} = 0$
$\nu_e - {}^{156}\text{Gd}$	9.5	15.22	81.55	0.61	0.46	0.04	0.37	1.68	0.02	200
$\nu_e - {}^{158}\text{Gd}$	9.5	17.46	78.86	0.63	0.45	0.06	0.54	1.93	0.02	224
$\nu_e - {}^{160}\text{Gd}$	9.5	19.58	77.50	0.61	0.43	0.04	0.60	1.15	0.02	241
$\bar{\nu}_e - {}^{156}\text{Gd}$	12	18.26	78.44	0.50	0.36	0.03	0.56	1.79	0.02	13.7
$\bar{\nu}_e - {}^{158}\text{Gd}$	12	19.14	77.46	0.58	0.38	0.05	0.81	1.51	0.02	9.7
$\bar{\nu}_e - {}^{160}\text{Gd}$	12	18.22	77.26	0.59	0.38	0.07	0.99	2.45	0.02	8.4

The flux-averaged supernova-neutrino ($SN - \nu$) cross sections, broken down by multipoles, appear in Table IV. The pinching parameter α has been taken the value $\alpha = 2.5$. As it is seen, at a typical supernova neutrino (antineutrino) mean energy $\langle E_{\nu_e} \rangle = 9.5 \text{ MeV}$ ($\langle E_{\bar{\nu}_e} \rangle = 12 \text{ MeV}$) the flux-averaged cross sections are dominated by the allowed (A) transition moments $J^\pi = 0^+, 1^+$ contributing about 97% of the total strength. The remaining part of the transition strength (3%) is carried almost entirely by the first forbidden (F1) moments $J^\pi = 1^-, 2^-$ and the second forbidden (F2): $J^\pi = 2^+, 3^+$. Moreover, in Fig.3 the cumulative flux-averaged cross section is illustrated as a function of the excitation energy ω for the reactions $\nu_e - {}^{160}\text{Gd}$ and $\bar{\nu}_e - {}^{160}\text{Gd}$. As it is seen, the dominant transitions lie to the energy region between 5-10 MeV. The region of maximum discontinuity of the cumulative cross sections coincides with the maximum multipole contribution of the 1^+ states, while, the shape of neutrino/antineutrino energy spectrum probes the giant resonance region of the nuclear spectrum where the cross sections vary quickly. The above results refer to an ideal detector operating down to zero threshold $E_{th} = 0$. In the case of non zero threshold the flux averaged cross sections will be suppressed. This is demonstrated in Fig. 4 where as an example the flux averaged cross sections for supernova neutrinos at $\langle E_{\nu_e} \rangle = 9.5 \text{ MeV}$ is plotted assuming a threshold E_{th} on the recoiling electron. As it is seen for an electron total energy threshold of 5 MeV (energy threshold in SK) the suppression to the flux flux-averaged cross section $\langle\sigma\rangle$ is about 9%.

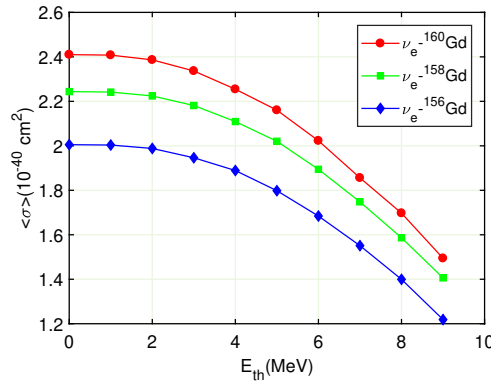


FIG. 4: (Color on line) Flux averaged cross sections (in units 10^{-40} cm^2) of supernova neutrinos at $\langle E_{\nu_e} \rangle = 9.5 \text{ MeV}$ as a function of energy threshold on the outgoing electrons.

Exploiting our predictions for the total cross sections $\nu - \text{Gd}$, the number of expected neutrino events are estimated in a WCD assuming the addition of 0.2% Gadolinium doping. Thus in the SK detector where the fiducial mass of water is 22.5 kton the Gadolinium mass there would be $m_t = 45 \text{ ton}$. A supernova radiates via neutrinos an amount of total energy $3 \times 10^{53} \text{ erg}$ in about 10 s . Assuming an equal partition of energy among neutrinos, the supernova radiates $N_{\nu_e} = 3.0 \times 10^{57}$ electron neutrinos and $N_{\bar{\nu}_e} = 2.6 \times 10^{57}$ electron antineutrinos. The neutrino fluence $\Phi(E_\nu)$

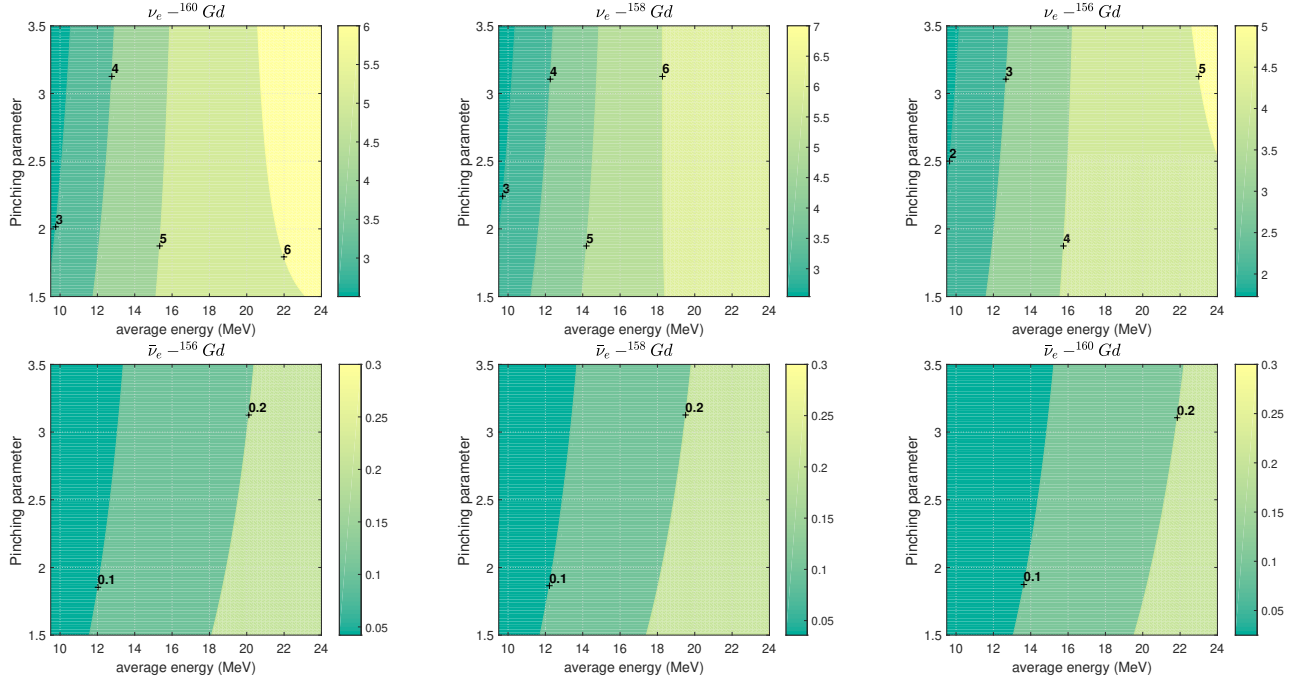


FIG. 5: (Color on line) These contour plots show the number of electrons (top panels) and positrons (bottom panels) emitted from 45 tons of Gd consisting of A=156,158 and 160 isotopes. The contours from left to right in each panel denotes the increase of the number of expected events. We have assumed a 5 MeV detection threshold.

for neutrinos integrated over 15 s burst is given by the relation

$$\Phi_i(E_\nu) = \frac{N_i}{4\pi D^2} \eta_{PL}(E_\nu), \quad i = \nu_e, \bar{\nu}_e \quad (9)$$

at a distance $D = 10 \text{ kpc} = 3.1 \times 10^{22} \text{ cm}$. If the mass of the target material is m_t , corresponding to N_t atoms then the number of expected events are

$$N_{event} = N_t \int \Phi_i(E_\nu) \sigma_i(E_\nu) dE_\nu = N_t \frac{N_i}{4\pi D^2} \langle \sigma_i \rangle \quad (10)$$

where $\langle \sigma_i \rangle$ the flux-averaged cross sections. In Fig. 5 a contour plot is used to display the number of expected events for the reactions $Gd(\nu_e, e^-)Tb$ and $Gd(\bar{\nu}_e, e^+)Eu$ respectively, with various parameterizations of power-law spectra. As it is seen, within a window of 10-18 MeV the number of events depends weakly on the pinching parameter α . However, at energies out of this region, the number of events increases faster.

Next the number of expected events in SK detector for a Galactic Supernova at 10kpc and for different values of the neutrino average energy are estimated in Table V. We consider 22.5 kton fiducial mass assuming a 100% tagging efficiency on expected events above the detection threshold. For comparison the detectable channels $\bar{\nu}_e + p$ (IBD), the elastic scattering $\nu_e + e^-$ (ES) as well as the neutral current scattering $\nu_e + {}^{16}\text{O}$ (OS) on oxygen are also calculated [30, 31]. Furthermore, in Fig. 6 it is shown the angular distributions of events as a function of scattering angle for the various detection channels. From the table, it is clear that the largest number of events will be due to the IBD which is almost isotropic [32], while the ES events spread out in a cone of about 20° [33] that points towards the neutrino direction (see Fig. 6a). Thus positrons from IBD and electrons from ES can be statistically distinguished by reducing the IBD background to the portion of the solid angle in which it overlaps to the ES signal. Beacom and Vagins [34] suggest that with 0.2% (by mass) Gd added to SK, $\sim 90\%$ of the IBD events could be tagged. The remaining IBD events as well as the $\bar{\nu}_e$ absorption events on ${}^{16}\text{O}$ can be statistically subtracted from the remaining signal. As it is clear from Table V the ν_e interactions on electrons are the largest in number among electron scattering interactions. Moreover, the ν_e -Gd charged current interactions as well as ES depend weakly on the average energy of the incoming neutrino. As it seen is from figure 3, ν_e -Gd events could be identified by the expected gamma lines in the energy window 5-10 MeV. The $\bar{\nu}_e$ -Gd interactions are quite small and are hidden by the large IBD interactions on free

TABLE V: Number of expected events in Super-Kamiokande for a Galactic supernova at a distance of 10 kpc for different values of averaged energy. The total energy of the supernova is assumed to be 3×10^{53} erg, equally partitioned among all flavors (here $\nu_x = \nu_\mu + \nu_\tau$ and $\bar{\nu}_x = \bar{\nu}_\mu + \bar{\nu}_\tau$). The detection threshold is taken 0 MeV (events in first parenthesis, 3 MeV (events in second parenthesis) and 5 MeV (events in third parenthesis). The pinching parameter α is taken 2.5. The fiducial mass of water that is being considered is 22.5kt with 45 tons of Gd.

Detection channel	9.5MeV	12MeV	15.6MeV	$N_t(10^{29})$
$\bar{\nu}_e + p \rightarrow e^+ + n$	(3231.39)(3210.18)(3108.87)	(4158.72)(4148.83)(4094.67)	(5404.75)(5400.84)(5376.67)	15000
$\nu_e + e^- \rightarrow \nu_e + e^-$	(178.24)(119.13)(85.53)	(179.45)(132.07) (103.49)	(180.53)(143.76)(120.69)	60000
$\bar{\nu}_e + e^- \rightarrow \bar{\nu}_e + e^-$	(75.59)(33.31)(19.38)	(75.97)(39.82)(25.97)	(76.30)(46.52)(33.51)	60000
$\nu_x + e^- \rightarrow \nu_x + e^-$	(60.12)(37.34)(25.99)	(60.18)(41.61)(31.69)	(60.22)(45.57)(37.30)	60000
$\bar{\nu}_x + e^- \rightarrow \bar{\nu}_x + e^-$	(51.97)(30.53)(20.74)	(51.96)(34.29)(25.54)	(51.94)(37.85)(30.39)	60000
$\nu_e + {}^{16}\text{O} \rightarrow \nu_e + {}^{16}\text{O}$	0.52	2.56	11.92	7500
$\bar{\nu}_e + {}^{16}\text{O} \rightarrow \bar{\nu}_e + {}^{16}\text{O}$	0.42	2.03	9.43	7500
$\nu_e + {}^{160}\text{Gd} \rightarrow e^- + {}^{160}\text{Tb}$	(2.81)(2.79)(2.72)	(3.89)(3.88)(3.80)	(5.07)(5.05)(4.97)	0.37
$\nu_e + {}^{158}\text{Gd} \rightarrow e^- + {}^{158}\text{Tb}$	(2.86)(2.85)(2.78)	(4.08)(4.06)(3.99)	(5.40)(5.38)5.31)	0.42
$\nu_e + {}^{156}\text{Gd} \rightarrow e^- + {}^{156}\text{Tb}$	(1.97)(1.97)(1.94)	(2.92)(2.90)(2.89)	(3.95)(3.94)(3.93)	0.35
$\nu_e + \text{Gd} \rightarrow e^- + \text{Tb}$	(7.64)(7.61)(7.44)	(10.89)(10.84)(10.68)	(14.42)(14.37)(14.21)	1.14
$\bar{\nu}_e + {}^{160}\text{Gd} \rightarrow e^+ + {}^{160}\text{Eu}$	(0.035)(0.033)(0.032)	(0.066)(0.066)(0.065)	(0.119)(0.120)(0.120)	0.37
$\bar{\nu}_e + {}^{158}\text{Gd} \rightarrow e^+ + {}^{158}\text{Eu}$	(0.046)(0.046)(0.045)	(0.086)(0.086)(0.084)	(0.147)(0.147)(0.143)	0.42
$\bar{\nu}_e + {}^{156}\text{Gd} \rightarrow e^+ + {}^{156}\text{Eu}$	(0.052)(0.052)(0.051)	(0.090)(0.090)0.090	(0.145)(0.145)(0.144)	0.35
$\bar{\nu}_e + \text{Gd} \rightarrow e^+ + \text{Eu}$	(0.133)(0.131)(0.128)	(0.242)(0.242)(0.239)	(0.411)(0.412)(0.407)	1.14

protons. As regards the OS signal [35], it is expected to be within $4 \div 9$ MeV, gamma lines cover the energy window $\approx 5.3 \div 7.3$ MeV. In this region it can not be disentangled from the many more IBD and ES background events. The

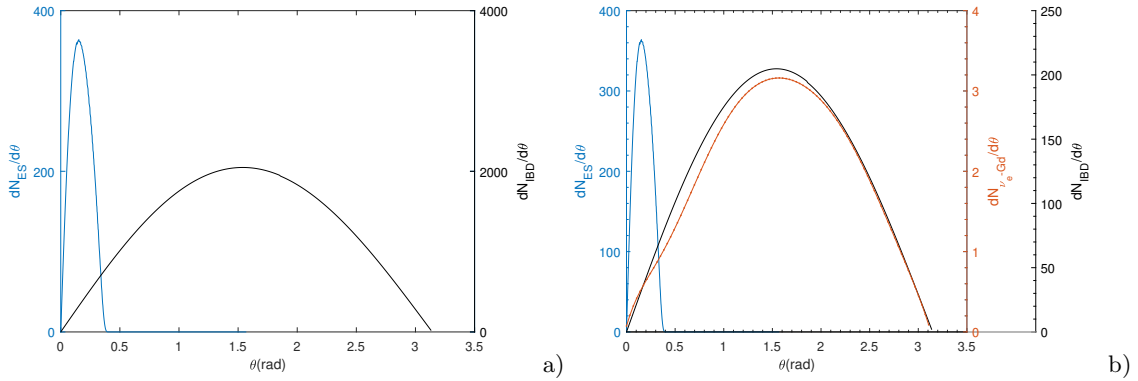


FIG. 6: (Color on line) Angular distributions of events for ES, IBD and ν_e -Gd as a function of the scattering angle θ without(left) or with Gd(right). We take $\langle E_{\nu_e} \rangle = 9.5\text{MeV}$ and $\langle E_{\bar{\nu}_e} \rangle = 12\text{MeV}$. We assume a Gd doping of 45 tons (0.2% in the fiducial water mass of 22.5 ktons). The energy threshold is taken 5 MeV.

main background for ES and ν_e -Gd interactions are the IBD events. Some of these numerous events can be removed using an angular cut but they still pose a formidable background (see Fig. 6a). Adding Gd to SK the inverse beta background will decrease about 90% (see Fig. 6b). This could improve the detection prospects of ES channel which is strongly forward peaked. The ability to cleanly isolate the dominant IBD events would be extremely important for studying the remaining reactions ν_e -Gd that lead to gamma emission. If ν_e -Gd events could be isolated either by gamma rays identification or by the determination of probable delayed beta decays, they might have some advantages due to the low thresholds (though low yields). Recently a new method was proposed [36] to introduce Gd-ions in WCDs, based to release of Gd-ions from custom designed glasses like those used for photomultiplier tube glass systems. This controlled Gd-ion release from a custom glass in the form of beads or powders may help in future WCDs to

enhance neutrino detection.

V. CONCLUSIONS

The addition of Gadolinium (Gd) salt in the Water Cherenkov Detectors (0.2% in SK) enhances the sensitivity to neutrino detection. In this work we have computed the cross sections for charged current neutrino and antineutrino scattering off the even $A=156-160$ (most abundant) Gd isotopes for energies relevant to supernova neutrinos. The neutrino induced transitions to excited nuclear states are computed in the framework of pnQRPA. The nuclear responses of the Gd isotopes for SN detection have been studied assuming a two-parameter quasi-thermal power law distribution. Our results show that the greatest part of responses comes from the excitation energy region $\omega < 20$ MeV. The neutrino-Gd channel have also been compared with three other channels, namely inverse beta decay, elastic scattering on electrons and neutral current scattering on oxygen. We tried to look at the angular dependence of the ν_e -Gd interaction signal in the SK detector with fiducial mass 22.5 kton of water and 0.2% Gd doping. The problem is the background of events from inverse beta channel. This background can be reduced for elastic scattering on electrons using an angular cut. The number of ν_e -Gd events are increasingly backward peaked and are about 40 times smaller than those of inverse beta events. It would be also interesting to investigate cross sections for charged current neutrino scattering off the odd $^{155,157}\text{Gd}$ isotopes. Detailed numerical results will be presented in a forthcoming paper. The sensitivity of the detectors, which is pivotal to the success of Water Cherenkov Detectors can be achieved including additives, such as Gd in water, something that is more financially sound and a less risky option than, either building a larger water tank or varying the size of photomultiplier tubes. The ability to a well understood reducible backgrounds above detector threshold is extremely important for studying charged current signals from supernova.

-
- [1] R. Becker-Szendy et al., Nucl. Instrum. Meth. A **324**, 363 (1993).
 - [2] Y. Fukuda et al., Nucl. Instrum. Meth. A **418**, 418 (2003).
 - [3] A. Bellerive, J. Klein, A. McDonald, A. Noble, and A. Poon, Nucl. Phys. B **908**, 30 (2016).
 - [4] R. Laha and J. F. Beacom, Phys.Rev. D **89**, 1 (2004).
 - [5] M. R. Vagins, Nucl.Phys.Proc.Suppl. **229-232**, 325 (2012).
 - [6] P. C. Divari, J. Phys. G: Nucl. Part. Phys. **40**, 125201 (2013).
 - [7] P. C. Divari, Advances in High Energy Physics **2013**, 143184 (2013).
 - [8] P. C. Divari, *Trends in Modern Cosmology* (InTech, 2017) Ed. A.J. Capistrano de Souza **Chapter 3**, p.47 (2017).
 - [9] R. Hemler, Nuclear Data Sheets **101**, 325 (2004).
 - [10] J. Walecka, *Theoretical Nuclear and Subnuclear Physics* (Oxford University Press, New York, 1995) p. 531 (1995).
 - [11] T. Donnelly and J. D. Walecka, Nucl. Phys. A **201**, 81 (1973).
 - [12] T. Donnelly and W. Haxton, At. Data and Nucl. Data Tables **23**, 103 (1979).
 - [13] T. Donnelly and R. Peccei, Phys. Rep **50**, 1 (1979).
 - [14] M. Athar, S. Ahmad, and S. Singh, Nucl. Phys. A **764**, 551 (2006).
 - [15] S. Singh, Nucl. Phys. B(Proc. Suppl.) **112**, 77 (2002).
 - [16] C. Lujan-Peschard, G. Pagliaroli, and F. Vissani, JCAP **1407**, 051 (2014).
 - [17] I. Tamborra, B. Muller, L. Hudepohl, H. Janka, and G. Raffelt, Phys. Rev. D **86**, 125031 (2012).
 - [18] M. T. Keil, G. G. Raffelt, and A.-T. Janka, Astrophys. J. **590**, 971 (2003).
 - [19] F. Vissani, J. Phys. G **42**, 27 (2005).
 - [20] M. L. Costantini, A. Ianni, and F. Vissani, Nucl. Phys. Proc. Suppl. **139**, 013001 (2015).
 - [21] A. Mirizzi, G. Raffelt, and P. Serpico, JCAP **0605**, 012 (2006).
 - [22] S. M. Adams, C. S. Kochanek, J. F. Beacom, M. R. Vagins, and K. Z. Stanek, Astrophys. J. **778**, 164 (2013).
 - [23] T. J. Loredo and D. Q. Lamb, Phys. Rev. D **65**, 063002 (2002).
 - [24] G. Pagliaroli, F. Vissani, M. L. Costantini, and A. Ianni, Astropart. Phys. **31**, 163 (2009).
 - [25] A. Bohr and B. R. Mottelson, *Nuclear structure* (Benjamin, New York, 1969).
 - [26] K. Holinde, Phys. Rep. **68**, 121 (1981).
 - [27] G. Audi et al., Nucl. Phys. A **729**, 337 (2003).
 - [28] M. Athar, S. Ahmad, and S. Singh, Phys. Lett. B **91**, 69 (2004).
 - [29] R. Lazauskas and C. Volpe, Nucl. Phys. A **792**, 219 (2007).
 - [30] R. Tomas, D. Semikoz, G. G. Raffelt, M. Kachelriess, and A. S. Dighe, Phys. Rev. D **68**, 093013 (2003).
 - [31] A. Strumia and F. Vissani, Phys. Lett. B **564**, 42 (2003).
 - [32] P. Vogel and J. F. Beacom, Phys. Rev. D **60**, 053003 (1999).

- [33] M. Nakahata et al., Nucl. Instrum. Meth. A **421**, 113 (1999).
- [34] J. F. Beacom and M. R. Vagins, Phys. Rev. Lett. **93**, 171101 (2004).
- [35] A. G. Rosso, F. Vissani, and M. C. Volpe, JCAP **4**, 40 (2018).
- [36] R. Dongol and S. Sundaram, Jinst **12**, 09028 (2017).